

Article

Study of the Convective Heat Transfer Coefficient of Different Building Envelope Exterior Surfaces

Xiaotong Xue ¹, Shouxu Han ¹, Dongjun Guo ^{2,*}, Ziwei Zhao ², Bin Zhou ¹ and Fei Li ^{1,*}¹ College of Urban Construction, Nanjing Tech University, Nanjing 211816, China;

xiaotongxue@njtech.edu.cn (X.X.); shouxuhan@njtech.edu.cn (S.H.); bin.zhou@njtech.edu.cn (B.Z.)

² Research Center for Underground Space, Army Engineering University of PLA, Nanjing 210007, China; ziiwei@163.com

* Correspondence: guo_dongjun@163.com (D.G.); faylee@njtech.edu.cn (F.L.)

Abstract: Convective heat transfer on the exterior surface of the building envelope is an important component for building energy consumption. The calculation of energy consumption depends on the convective heat transfer coefficient (CHTC) of the exterior surface of the envelope. The existing research does not fully consider the effects of the airflow field around the building on the CHTC of different envelope exterior surfaces. In this paper, the relationships between the CHTC and influence factors were investigated for the isolated building. Response surface methodology (RSM) and support vector machine (SVM) algorithms were integrated with the single building simulation to build the fitting formulas. Then, the fitting correlation between CHTC and different influencing factors was validated by the heating building simulation. The results showed that the CHTC of the building exterior surface was related to the wind velocity, wind direction and temperature difference. Additionally, the fitting formulas had good accuracy in calculating the CHTC under different conditions. The SVM algorithm (averaged error: 3.34%) performed slightly better than the RSM algorithm (averaged error: 4.84%).



Citation: Xue, X.; Han, S.; Guo, D.; Zhao, Z.; Zhou, B.; Li, F. Study of the Convective Heat Transfer Coefficient of Different Building Envelope Exterior Surfaces. *Buildings* **2022**, *12*, 860. <https://doi.org/10.3390/buildings12060860>

Academic Editor: Cinzia Buratti

Received: 16 May 2022

Accepted: 14 June 2022

Published: 20 June 2022

Publisher's Note: MDPI stays neutral with regard to jurisdictional claims in published maps and institutional affiliations.



Copyright: © 2022 by the authors. Licensee MDPI, Basel, Switzerland. This article is an open access article distributed under the terms and conditions of the Creative Commons Attribution (CC BY) license (<https://creativecommons.org/licenses/by/4.0/>).

Keywords: energy consumption; CFD; fitting correlation; SVM; wind environment simulation

1. Introduction

The energy load on the outer surface of a building envelope is related to the overall energy demand of the building. Research related to this subject is of great significance because it is relevant to energy savings and environmental protection [1,2]. On the outer surface of a building envelope, heat transfer occurs through convection and radiation processes. The radiant heat transfer is a function of surface temperature and emissivity and can be calculated directly. While the convective heat transfer is a function of many variables, such as temperature, wind velocity and direction of the wind, which makes it difficult to accurately determine the heat exchange properties of a building [3–5]. More study of the CHTC of the outer surface is necessary.

At present, the methods used to research CHTC of exterior surfaces of building envelopes mainly include laboratory-scale experiments and field full-size experiments in field trials. The formula used for the calculation of CHTC was obtained from a statistical study of experimental data. First, the studies which determined the formula of the CHTC based on wind tunnel experimental data are introduced. The formula proposed by McAdams was based on the results of a wind tunnel experiment reported by Jurges: $h = 5.678 \left[m + n \left(\frac{V_f}{0.3048} \right)^p \right]$ [6,7], where V_f is the wind velocity away from an object or physical boundary. The formula proposed in the Chartered Institute of Building Services (CIBS) Guide was also based on the results of the wind tunnel experiment reported by Jurges: $h = 4.1V_{loc} + 5.8$ [7], where V_{loc} is the wind velocity measured at a certain distance D from the front of the building and a certain height H from the ground. The Building

Loads Analysis and System Thermodynamics (BLAST) calculation formula was based on the results of a wind tunnel experiment conducted by Sparrow et al. [8]. It clearly distinguished forced convection from natural convection and modeled the total CHTC as the sum of natural and forced components of convection: $h_c = h_{c, nat} + h_{c, for}$.

Second, a calculation formula was introduced for the CHTC based on full-size experimental data was introduced. The formula proposed by Jayamaha et al. [9], was derived from field measurements using a freestanding aluminum plate (1.8 m × 1.2 m) mounted in the center of a large plywood sheet and shielded from direct solar radiation by an opaque shield: $h = 1.444V + 4.955$. The formula proposed by Sturrock was based on field measurements using a Ni-Cr strip on a 26 m high building [10]. The formula for an exposed surface was $h = 6.1V_R + 11.4$, and the formula for a normal surface was $h = 6V_R + 5.7$, where V_R is the wind velocity measured from the height of the roof surface. The ASHRAE task group's formula was based on the results of Ito et al. [11], who conducted an experiment on the front of an L-shaped building in Tokyo: $h = 18.6V_{loc}^{0.605}$, where V_{loc} is the wind velocity measured at a certain distance D from the front of the building and a certain height H from the ground. The formula proposed by Nicol was based on measurements in the field at night for an outer window in the Canadian Arctic region: $h = 7.55V + 4.35$, $0 < V < 5$ m/s [12], where V is the roof wind velocity. The formula proposed by Yazdani and Klems was: $h = \sqrt{\left(C_t(T_s - T_a)^{\frac{1}{3}}\right)^2 + (aV^b)^2}$ [13], where V is the wind velocity measured 10 m above the ground. The formula proposed by Loveday and Taki was based on measurements of a full-size building with eight stories and a total height of 28 m in a semiurban environment [14]. The formulas were $h = 16.15V_{loc}^{0.397}$, for the leeward sides and the $h = 16.25V_{loc}^{0.503}$, for the leeward sides where V_{loc} is the wind velocity measured at a certain distance D from the front of the building and a certain height H from the ground. The formula proposed by Hagishima and Tanimoto was based on a test conducted on a two-story building [15]. The formula for the horizontal plane was $h = 2.28V_R + 8.18$, and that for the vertical plane was $h = 10.21V_{loc} + 4.47$, where V_R is the wind velocity measured at the height of the roof surface, and V_{loc} is the wind velocity measured at a certain distance D from the front of the building and a certain height H from the ground. Most of the formulas used in current studies for the calculation of the CHTC mentioned above are based on the statistical analysis of experimental data, which are very limited for this application and do not comprehensively consider factors such as wind velocity, wind direction and temperature difference.

More recently, computational fluid dynamics has also been used to predict convective heat transfer on building surfaces because of its ability to analyze complex built environments and obtain high-resolution data [16]. Defraeye et al. evaluated the CHTC on the exterior surfaces for an incidence angle of 0° (wind direction perpendicular to one of the surfaces) and found the accurate CHTC could be obtained with low-Reynolds number modelling (LRNM) simulation [17]. Fakhim et al. investigated the impact of multiple parameters [18], namely temperature difference, wind speed, and wind direction on CHTC, all the correlations used in EnergyPlus software for the exterior surface of the building were compared with simulated data. Although wind direction was considered in above two studies, the first study required an incidence angle of 0° , and the second study only considered the windward and top sides. In addition, Chen et al. conducted continuous measurements of CO₂, TVOC and HCHO in five rooms [19], and analyzed the data correlation by four methods including support vector machine (SVM), Gaussian processes, M5P and backpropagation. Overall, SVM scored the highest. Yi et al., quantitatively investigated the relationship between the air change rate of naturally ventilated dairy buildings by RSM and CFD simulation [20]. The above research reported that RSM and SVM algorithms have good performance in data fitting.

In this study, CFD simulations combined with response surface method (RSM) and support vector machine (SVM) algorithms were used to research the relationship between the CHTC of the building envelop and the influence factors such as wind velocity, wind

direction and temperature difference. Additionally, the fitting formulas for the CHTC of different envelope exterior surfaces under different airflow field conditions were determined. The specific steps were as follows: first, CFD simulations were carried out for a single building and a heating building to verify the numerical model; second, the verified CFD model was used to conduct the single building simulations for cases under different conditions to obtain the necessary data for the fitting formulas; third, these simulation data were combined with RSM and SVM algorithms to obtain the fitting formulas of the CHTC on different envelope exterior surfaces; and finally, the fitting results of RSM and SVM algorithms were compared.

2. Methodology

The single building simulation was first used to establish the fitting formulas. In the simulation cases, the wind velocity and heat flux data on different envelope exterior surfaces were exported directly, and these data were used to fit the parameters of the dimensionless equation. Then, the heating building simulation was used to validate the fitting formulas.

2.1. Numerical Analysis

2.1.1. Single Building Simulation

The case study used in this research was the wind tunnel experiment of Tominaga et al. [21]. The experiment was well equipped and completed, and the experimental data obtained from the experiment were relatively complete. In addition, CFD simulation could be used for reference, and there was a good consistency between the data from experiment and simulation.

The details of the model of the experimental wind tunnel were as follows. First, a cubic model with a height of 0.2 m was set in the turbulent boundary layer, as shown in Figure 1. The external dimensions of the model building were 0.2 m (length) \times 0.2 m (width) \times 0.2 m (height) [22]. Second, the outlet for pollutants was a square, and the side length of the outlet was set as 0.005 m; it was located on the ground in the recirculation area behind the cube and 0.1 m away from the leeward wall of the building. The release velocity of the outlet gas was half of the inflow velocity on the inflow boundary.

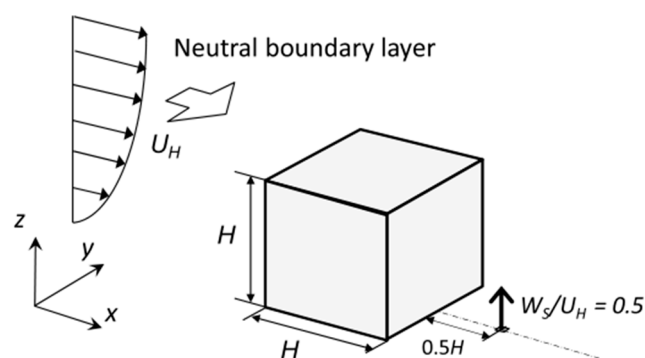


Figure 1. Single building model (Tominaga et al. [21]).

Numerical Method

As shown in Figure 2, the computational domain was sufficiently large to ensure that the calculation results were independent of the domain inlet boundary. The lateral boundary and the top boundary were set at 5 H from the building, and the flow boundary was set at 15 H from the building [22], where H was the height of the single building. Therefore, the length, width, and height of the computational domain were set to 21 times, 11 times and 6 times the building height, respectively. The length, width, and height of the computational domain were set to 4.2 m, 2.2 m, and 1.2 m.

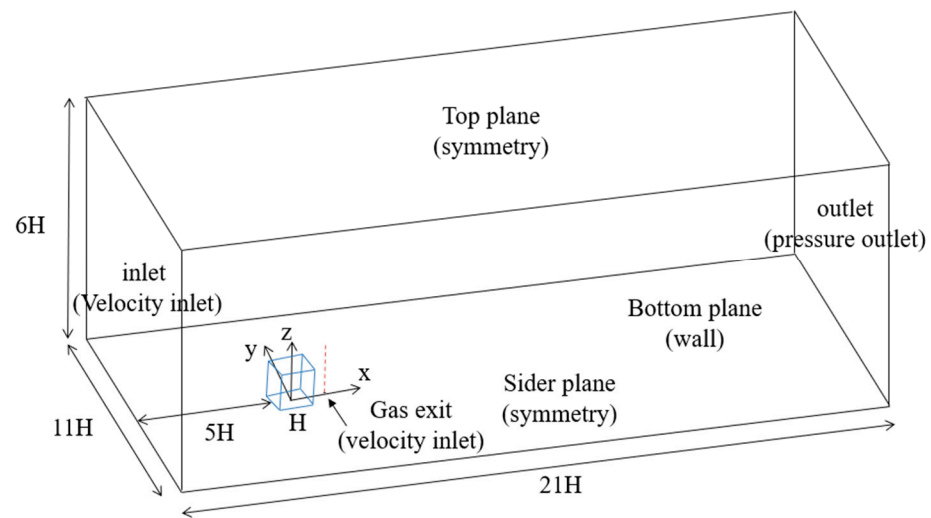


Figure 2. Computational domain and boundary conditions of the single building case.

For this case, the standard $k-\epsilon$ model [22], which performed well in simulation of flow structures and was typically used to simulate turbulent flows, and the enhanced wall function were used in this study. This turbulence model could provide reasonable solutions to a wide range of flow, heat, and pollutant transport problems while requiring relatively low computational costs. The buoyancy caused by the thermal effect was also considered in this work. We use a uniform formula to generalize the standard $k-\epsilon$ model:

$$\frac{\partial(\rho\varnothing)}{\partial t} + \text{div}(\rho\vec{u}\varnothing) = \text{div}(\Gamma_{\varnothing,eff}\cdot\text{grad}\varnothing) + S_{\varnothing} \quad (1)$$

where \varnothing presents the variables (velocity, enthalpy, turbulence parameters and concentration), $\Gamma_{\varnothing,eff}$ the effective diffusion coefficient, S_{\varnothing} the source term, and \vec{u} the Reynolds-averaged velocity vector. Details about the terms and coefficients for the different variable can be found in the Ansys theory guide (Ansys, 2019) [23].

The Prandtl number (Pr) of the wall was set to 0.1. The vertical velocity profile of the inflow boundary was modeled by a power law, the index α was set as 0.25, and the boundary velocity assignment equation was:

$$U_z = U_r \left(\frac{z}{z_r} \right)^\alpha \quad (2)$$

where U_r (m/s) is the velocity at the reference height z_r (m). The pollutant release velocity was set as 0.2 m/s. The turbulent kinetic energy was set to $0.002 \text{ m}^2/\text{s}^2$, and the turbulent dissipation rate was set to $0.042 \text{ m}^2/\text{s}^3$. The reference height was set to 0.2 m, and the reference velocity was set to 0.4 m/s. The computational domain's grid was set to $183 (x) \times 121 (y) \times 61 (z)$ (approximately 1.35 million) [21].

Validation of the Numerical Method

Figures 3 and 4 show the comparison results of the CFD model of the single building. The two graphs compare the simulated and experimental data for normalized velocity and normalized pollutant concentration, respectively. H is the building height, U_H is the reference wind velocity, x and z are the horizontal and vertical coordinates, and c_0 is the reference concentration:

$$c_0 = \frac{Q_e}{H^2 U_H} \quad (3)$$

where Q_e is the pollutant release velocity. The simulation results are in good agreement with the data from the wind tunnel experiment. From the figures, the predicted values

agree well with the experimental data. Therefore, the numerical calculation model can be used to calculate the numerical cases which were required for the fitting formulas of the CHTC.

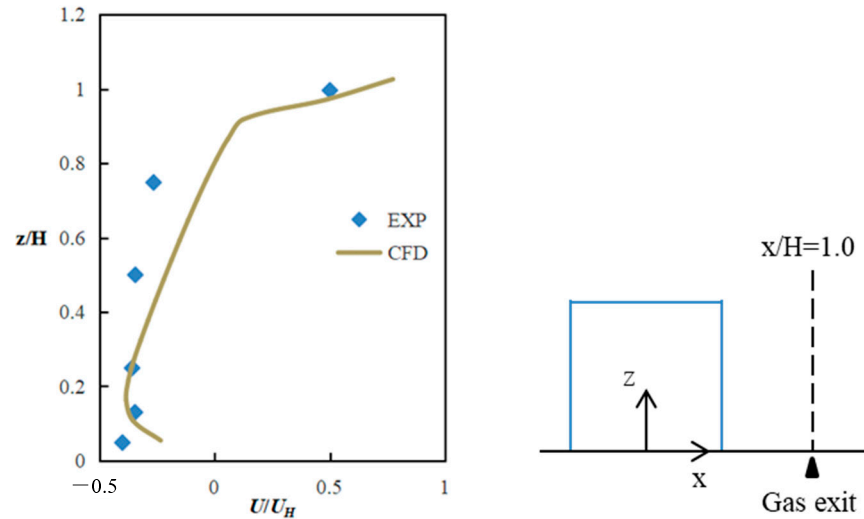


Figure 3. Comparison of the normalized wind velocity at a center section ($y/H = 0$).

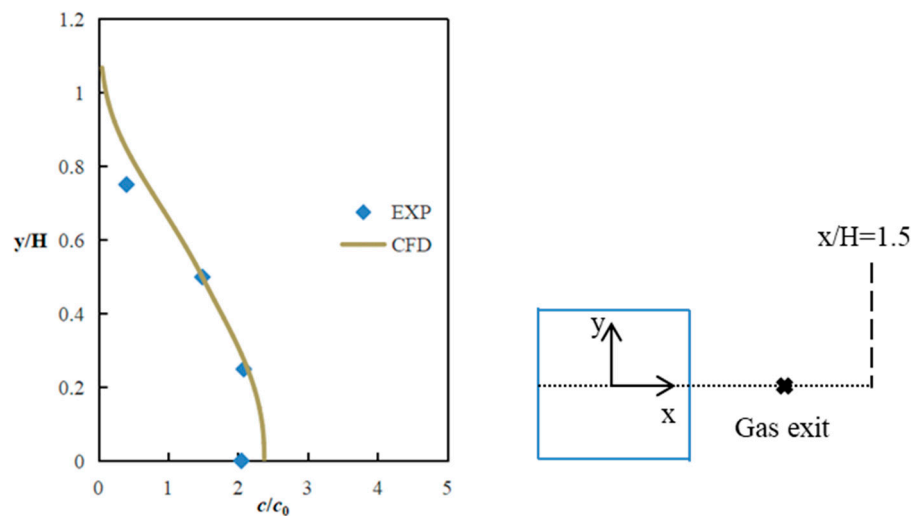


Figure 4. Comparison of the normalized pollutant concentrations at horizontal profiles at a half building height ($z/H = 0.5$).

CFD Simulation Cases for Building the Fitting Formulas

Based on the validated numerical method, more cases were conducted to analyze the fitting the relationship between the CHTC and influencing factors. Boundary conditions were set to meet the new case requirement, such as different velocities, temperature differences and wind directions. In addition, the selection range of different wind velocities needed to cover the airflow conditions from natural convection to forced convection. As preferred, most of the wind velocities were in the range of the mixed convection state. The evaluation of the mixed convection state was based on the comparison of buoyancy and inertial forces. The specific mathematical expression was as follows:

$$\frac{Gr}{Re^2} = \frac{g\alpha_v\Delta t l^3}{v^2} \frac{v^2}{u^2 l^2} = \frac{g\alpha_v\Delta t l}{u^2} \quad (4)$$

It was generally believed that when $\frac{Gr}{Re^2} < 0.1$, the flow field was mainly in a forced convection state; when $\frac{Gr}{Re^2} \geq 10$, the flow field was mainly a natural convection state. When $0.1 \leq \frac{Gr}{Re^2} \leq 10$, the flow field was mainly mixed convection. For the relevant values in the above formula, $g = 9.8 \text{ m/s}$ and $\alpha_v = 3.676 \times 10^{-3} \text{ K}^{-1}$ were calculated when $\frac{Gr}{Re^2}$ was 0.1 and 10, respectively. The calculated u values were $0.6\sqrt{\Delta t l}$ and $0.06\sqrt{\Delta t l}$. Therefore, when $u > 0.6\sqrt{\Delta t l}$, the flow state of the flow field was mainly forced convection; when $u \leq 0.06\sqrt{\Delta t l}$, the flow state of the flow field was mainly natural convection. When $0.06\sqrt{\Delta t l} \leq u \leq 0.6\sqrt{\Delta t l}$, the flow state of the flow field was mainly mixed convection. Table 1 shows the wind velocity range corresponding to the three flow states of the flow field.

Table 1. Wind velocity ranges and flow regimes.

Wind Velocity Range	$u \leq 0.06\sqrt{\Delta t l}$	$0.06\sqrt{\Delta t l} \leq u \leq 0.6\sqrt{\Delta t l}$	$u > 0.6\sqrt{\Delta t l}$
Flow regime	Natural convection	Mixed convection	Forced convection

This study selected six different wind velocities, three different wind directions and three different temperature differences between the outer surface of the building envelope and the surrounding environment. The specific settings of all different boundary conditions are shown in Table 2. As shown in the table, there were 54 cases. The relevant setting was the same as the isolated building case in Section Numerical Method. In these cases, the Boussinesq approximation was used for air thermal buoyancy due to the temperature difference. Finally, 234 sets of simulation data were used to fit the formulas for the calculation of the CHTC on the exterior surface of the building envelope.

Table 2. Boundary conditions.

Wind Velocity/m/s	Wind Direction Angle/°	Temperature Difference/K
0.2	0	1
0.4		
0.6		
0.8	30	2
1		
1.2		
	45	3

2.1.2. Heating Building Simulation

A CFD simulation of the flow and temperature fields of another building heated on the leeward side and near the ground was carried out. The predicted data were used to verify the fitting formulas of CHTC obtained from Section 2.1.1.

The wind tunnel experiment of Huang et al. [24] was selected. In their study, the wind tunnel model was composed of a cuboid building of L (length) \times L (width) \times $3L/2$ (height), where $L = 0.2 \text{ m}$. A cylindrical chimney with an internal diameter of 0.007 m and a height of $L/6$ was in the center of the building. The entrance velocity vector was perpendicular to the windward side of the building. The leeward side and adjacent ground were heated to simulate solar radiation.

Numerical Method

As shown in Figure 5, this study used the symmetry computational domain, and the scale of numerical model was only half of the wind tunnel experimental model. The entrance, lateral and top boundaries were set at $15L/2$ away from the building, and the outflow boundary was set at $45L/2$ behind the building. This computational domain was large enough and ensured the computational results were independent of the domain

size. The computational grid was set to $320 (x) \times 144 (y) \times 80 (z)$ [24] (approximately 3.69 million).

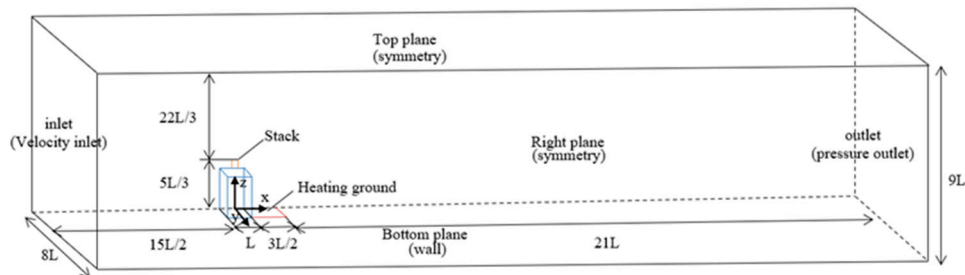


Figure 5. Computational domain and boundary conditions of the heating building case.

For this case, we also used the standard $k-\epsilon$ model and the standard wall function [22]. The vertical velocity profile at the inflow boundary was modeled as a power law, and the index α was set to 0.25, the reference height was set to 0.3 m, and the reference velocity was set to 3 m/s. The turbulent kinetic energy was set to $0.002 \text{ m}^2/\text{s}^3$, and the turbulent dissipation rate was set to $0.042 \text{ m}^2/\text{s}^3$. The temperature on the leeward side of the building and adjacent ground was set to 423 K, and the air temperature was set to 303 K. The governing equations for the turbulence models were the same as those described in Section Numerical Method. The solution settings were the same as those described in Section Numerical Method. In addition, the relative residual of energy equation was set to less than 10^{-7} .

Validation of the Numerical Method

Figures 6 and 7 show the verification results of the heating building simulation case. These three graphs compare the simulated and experimental data for normalized velocity and normalized temperature. H is the building height ($H = 3L/2$), T_0 is the operating temperature, U_H is the reference wind velocity. The simulation results are in good agreement with the wind tunnel experimental data. The data from this case can be used to verify the fitting formulas of the CHTC.

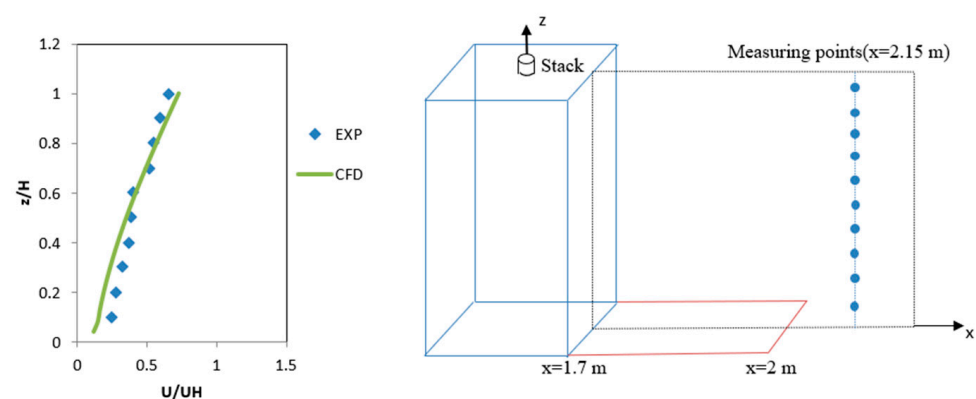


Figure 6. Velocity measuring points on the $y = 0 \text{ m}$ plane.

Validation Cases for the Fitting Formulas

The setting of different boundary conditions is needed to cover different velocities and different temperature differences. In addition, to meet the requirements of Reynolds independence and ensure the similarity of the flow field structure, the Reynolds number should be greater than 11,000. When the wind velocity is 1.5 m/s, 3 m/s or 4.5 m/s, the Reynolds numbers of the cases are greater than 11,000 and met the requirements of Reynolds independence and structural similarity of the flow field. Therefore, three different

wind velocities and temperature differences between the building surface and air were selected in this study. As shown in Table 3, there were 9 validation cases used to verify the fitting formulas of the CHTC on the exterior surface of the building envelope. The relevant numerical settings were the same as Section Numerical Method.

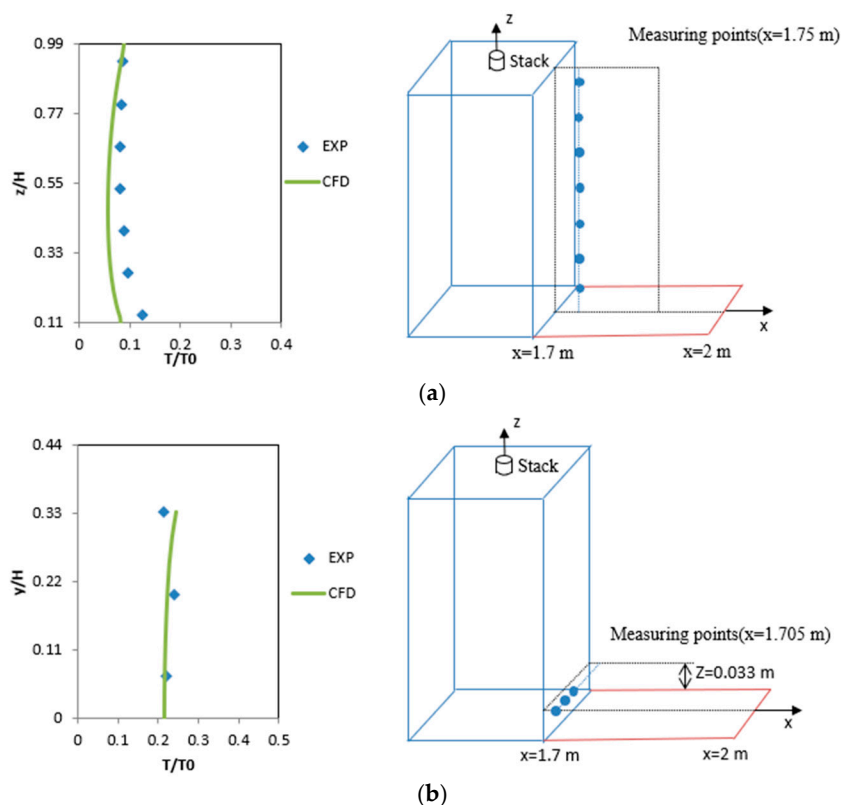


Figure 7. Temperature measuring points on the planes of (a) $y = 0$ m and (b) $z = 0.033$ m.

Table 3. Sets of different boundary conditions.

Inflow Wind Velocity/m/s	Temperature Difference/K
1.5	40
3	80
4.5	120

2.2. Response Surface Methodology

RSM is a data fitting method. When a certain amount of relevant experimental data through several groups of actual experiments are obtained, multiple quadratic regression equations are used to fit the numerical relationship (also called the functional relationship) between the impact factors and the response values. RSM approximates the implicit limit state function with polynomial functions, and the optimal fitting parameters can be determined to solve the mathematical problems of multiple influencing factors. To ensure that the polynomial function converges, the reasonable selection of test points and iterative correlation strategies are important. When the actual limit state function is linear, the linear response surface method has higher approximate accuracy than other methods. The mathematical model $y = f(x_1, x_2, \dots, x_n) + e$ is used to determine the relationship between y and its influencing factors (x_1, x_2, \dots, x_n) [24], where the error value of the model

is represented by e . In this study, the above model is expressed as a quadratic Taylor series polynomial function, as shown in Equation (8).

$$y = \beta_0 + \sum_{i=1}^n \beta_i x_i + \sum_{i=1}^n \beta_{ii} x_i^2 + \sum_{i=1}^{n-1} \sum_{j>i}^n \beta_{ij} x_i x_j + e \quad (5)$$

where y is the dependent variable; x_i and x_j are independent variables; n is the number of independent variables; β_0 , β_i , β_{ii} and β_{ij} are regression coefficients; and e is the error value. The general procedure for developing polynomial approximations using the RSM is as follows:

- (1) Experimental design. The relationship between dependent variables and independent variables is clarified according to the research purpose. The range of independent variables was determined. Then, appropriate methods are used to determine the permutations and combinations of the values of a series of independent variables.
- (2) Acquisition of response data. Response data are obtained through experiment or simulation.
- (3) Establishment of response surface model. The experimental or simulation results are used to fit to a suitable mathematical model, and the correlation coefficient of the model is determined by regression analysis.

In this study, the CFD simulation of the flow and temperature fields was conducted to produce relevant response data. The response data were then grouped and numbered. The fitting toolbox in MATLAB was used to fit the response data of different groups, and the response surface models were obtained for Nu (Nusselt number), Gr (Grashkov number) and Re (Reynolds number). Finally, the fitting formulas of the CHTC were obtained.

2.3. Support Vector Machine

SVM [25] is a generalized linear classifier that classifies binary data through supervised learning, and it follows the principle of minimizing structural risk. To optimize the structural risk, a regularization term is added to the solution system. Based on the limited sample information, SVM method can identify random samples correctly and have optimal generalization ability. It uses the hinge loss function to calculate empirical risk. The basic idea of SVM is to map the original training sample x_i to a higher dimensional space through a nonlinear mapping function ϕ . Then, a linear classification hyperplane with the largest boundary is found in the high-dimension space. Given a set of training samples (x_i, y_i) , including $x_i \in R^n$, $y_i \in \{1, -1\}^l$, and $i = 1, \dots, l$, the basic functions of SVM are as follows:

$$\begin{aligned} \min_{w,b,\zeta} \quad & \frac{1}{2} w^T w + C \sum_{i=1}^l \zeta_i \\ \text{subject to} \quad & y_i (w^T \phi(x_i) + b) \geq 1 - \zeta_i \\ & \zeta_i \geq 0 \end{aligned} \quad (6)$$

where C is the penalty parameter (greater than 0), w is the normal vector of the hyperplane, b is the intercept of the hyperplane, and ζ_i is the relaxation variable. Because SVM applies the kernel expansion theorem, it is not necessary for it to know the exact expression for the nonlinear mapping ϕ . In addition, because SVM applies the method of linear learning to the feature space of high dimensions through a kernel function, compared with linear models, it avoids the adverse effects of high-dimensional calculations to some extent. The most commonly used kernel function of SVM is the radial basis function (RBF), and its specific form is as follows:

$$K(x_i, x_j) = \gamma (x_i^T x_j + r)^d, \gamma > 0 \quad (7)$$

where r , d , and γ are kernel parameters. For RBF, the prediction accuracy depends on the optimization setting of penalty parameter C and kernel parameter γ , and the choice of

optimal values for these two parameters requires careful consideration. The method of cross validation [26] is always chosen to obtain the optimal values of C and γ .

3. Results

3.1. Correlation of the Convective Heat Transfer Coefficients

In the CFD simulation cases, the heat flux on different envelope exterior surfaces were exported to calculate their corresponding convective heat transfer coefficients, the wind velocity outside the top boundary layer of the building was employed, and characteristics length was set as the building height. Based on these data, we obtained 234 sets of Nu , Gr , and Re values. Nusselt Number was calculated for each target surface. These data were used to fit the parameters of the dimensionless equations associated with the CHTC as follows:

$$Nu = cRe^m Gr^n Pr^0 \quad (8)$$

For RSM, the polynomial fitting method was adopted in this study, and the relationship between simulated data was logarithmic as follows:

$$\ln Nu = \ln C + m \ln Gr + n \ln Re \quad (9)$$

The fitting formulas for calculating the CHTC on the exterior surface of the building envelope at different wind angles could be divided into several categories. For the 0° wind direction condition, the CHTC of the side and top surfaces the building could be grouped together. While the convective heat transfer coefficients on the windward and leeward sides should be treated separately. Based on the fitting calculation, the CHTC of the windward side under 30 and 45° wind direction conditions could be grouped in one category. However, the coefficients of different leeward sides should be treated separately. In addition, the CHTC under the 60° wind direction condition could be calculated by referring to the results under the 30° wind direction. The results are shown in Tables 4 and 5.

Table 4. RSM fitting formulas under the 0° wind direction condition.

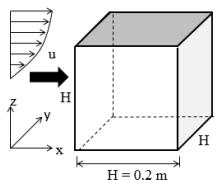
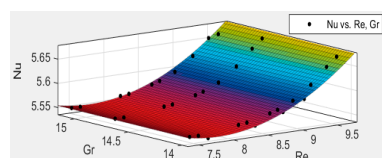
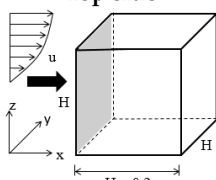
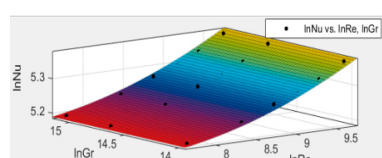
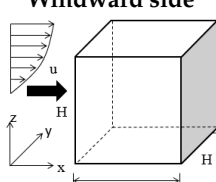
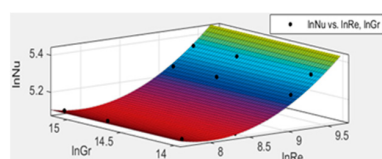
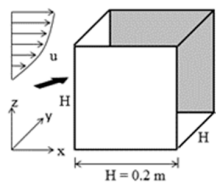
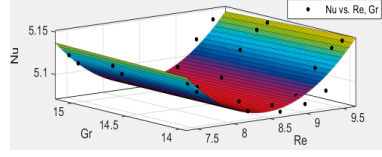
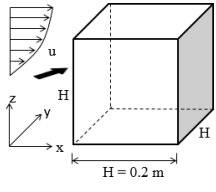
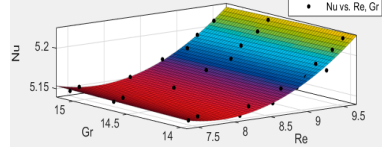
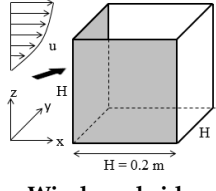
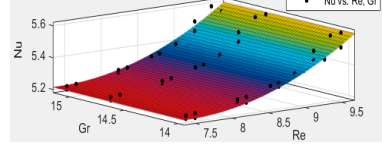
Surface	Response Surface Model	R-Square	Predicted
	$\begin{aligned} \ln Nu &= 7.463 - 0.5098 \ln Re \\ &+ 0.008807 \ln Gr \\ &+ 0.03375 (\ln Re)^2 \\ &- 0.001067 \ln Re \ln Gr \end{aligned}$	0.9619	
Top side 	$\begin{aligned} \ln Nu &= 6.222 - 0.3110 \ln Re \\ &+ 0.00007340 \ln Gr \\ &+ 0.02304 (\ln Re)^2 \\ &- 0.000007894 \ln Re \ln Gr \end{aligned}$	0.9978	
Windward side 	$\begin{aligned} \ln Nu &= 13.52 - 2.102 \ln Re \\ &- 0.003229 \ln Gr \\ &+ 0.1308 (\ln Re)^2 \\ &+ 0.0004581 \ln Re \ln Gr \end{aligned}$	0.9789	
Lee side			

Table 5. RSM fitting formulas under the 30° and 45° wind direction condition.

Surface	Response Surface Model	R-Square	Predicted
 <p>Lee side 1</p>	$\begin{aligned} \ln Nu &= 7.954 - 0.7279 \ln Re \\ &+ 0.02842 \ln Gr \\ &+ 0.04606 (\ln Re)^2 \\ &- 0.003473 \ln Re \ln Gr \end{aligned}$	0.7154	
 <p>Lee side 2</p>	$\begin{aligned} \ln Nu &= 6.255 - 0.3253 \ln Re \\ &+ 0.02174 \ln Gr \\ &+ 0.02311 (\ln Re)^2 \\ &- 0.002593 \ln Re \ln Gr \end{aligned}$	0.9304	
 <p>Windward side</p>	$\begin{aligned} \ln Nu &= 8.809 - 1.037 \ln Re \\ &+ 0.03020 \ln Gr \\ &+ 0.07366 (\ln Re)^2 \\ &- 0.003685 \ln Re \ln Gr \end{aligned}$	0.9411	

For SVM, the CFD simulation data were divided into six groups and converted into libsvm data format [26]. Then, the six groups of sample data were scaled to obtain six groups of training sample sets, and the scaling interval was set as [−1, +1]. This study chose the RBF kernel as the kernel function. Six different penalty parameter C and kernel parameter γ were obtained by cross-validation based on six groups of test sample data. Finally, the SVM predictions for the six groups of sample datasets were obtained as shown in Tables 6 and 7.

Table 6. SVM fitting models under the 0° wind direction condition.

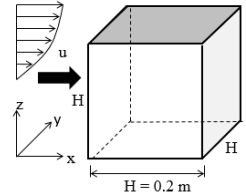
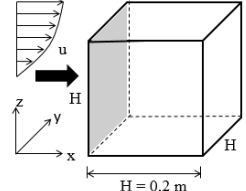
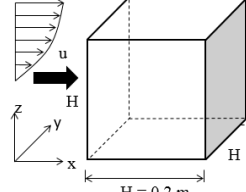
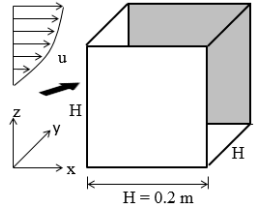
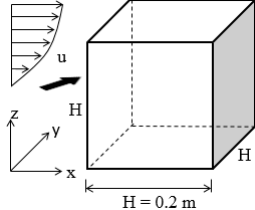
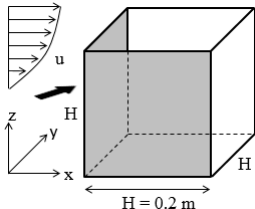
Surface	Accuracy	Best C, Gamma	Surface
Top side	100%	2, 2	
Windward side	72.22%	2, 8	
Lee side	61.11%	32, 0.5	

Table 7. SVM fitting models under the 30° and 45° wind direction condition.

Surface	Accuracy	Best C, Gamma	Surface
Lee side 1	91.67%	32, 0.5	
Lee side 2	86.11%	2, 8	
Windward side	98.61%	8, 2	

3.2. Validation of the Fitting Formulas

We further validated the fitting formulas by using CFD simulation data of the flow and temperature fields of heating building simulation in Section Validation Cases for the Fitting Formulas. As the heating building simulation was conducted under the 0° wind direction, the fitting formula for the leeward side of the building under the 0° wind direction was selected for verification in this study.

The selected fitting formula for the leeward side of the building under the 0° wind direction is as follows:

$$\ln Nu = 13.52 - 2.102 \ln Re - 0.003229 \ln Gr + 0.1308 (\ln Re)^2 + 0.0004581 \ln Re \ln Gr \quad (10)$$

The CFD predicted value of $\ln Nu$ can be calculated as follows:

$$\ln Nu = \ln \frac{hl}{\lambda} = \ln \frac{ql}{\Delta t \lambda} \quad (11)$$

The calculation error e can be expressed as:

$$e = \left| \frac{\text{CFD simulation value} - \text{Fitting value}}{\text{CFD simulation value}} \right| \times 100\% \quad (12)$$

Table 8 shows the comparison of the simulated values and fitting values. From the table, the fitting model based on the single building simulation can predict the CHTC of the heating building under different airflow velocities and temperature differences. The calculation errors were almost below 10%, and compared with RSM (averaged error: 4.84%), the accuracy of SVM (averaged error: 3.34%) was slightly higher. In addition, this study only employed the isolated building cases to build and validate the fitting model, and further real-world experiments are needed to test and improve the fitting model.

Table 8. Verification results of the fitting models.

u2/m/s, Δt/K	CFD Simulation Value	RSM Fitted Value	SVM Fitted Value	Error	
				RSM	SVM
3, 120	5.838	6.261	5.597	7.25%	4.13%
3, 80	5.867	6.260	5.584	6.70%	4.82%
3, 40	5.969	6.259	5.578	4.86%	6.55%
1.5, 120	5.767	5.736	5.759	0.54%	0.14%
1.5, 80	5.782	5.735	5.750	0.81%	0.55%
1.5, 40	5.664	5.734	5.739	1.24%	1.32%
4.5, 120	6.128	6.570	5.872	7.21%	4.18%
4.5, 80	6.113	6.569	5.858	7.46%	4.17%
4.5, 40	6.109	6.568	5.851	7.51%	4.22%

4. Conclusions

In this paper, the correlation between the CHTC and influencing factors for different exterior surfaces of the isolated building was investigated. We used CFD simulation of a single building to obtain 234 sets of simulation data including the values of Nu, Re and Gr, which were used to fit the parameters of the dimensionless equations by RSM and SVM algorithms. The results showed that the CHTC of the building exterior surface was related to the wind velocity, wind direction and temperature difference, and the errors of RSM and SVM were approximately 4.84 and 3.34%, respectively. It indicated that the fitting formulas based on RSM and SVM had good performance in calculating the CHTC under different conditions for the isolated building. However, in this study, we only investigated the fitting formula of CHTC on isolated building surfaces. In the future, the cases in which the building is surrounded by shelter or located in a group of buildings will be studied.

Author Contributions: Conceptualization, F.L. and D.G.; methodology, F.L. and S.H.; validation, S.H.; formal analysis, X.X.; investigation, S.H.; resources, D.G. and Z.Z.; data curation, B.Z.; writing—original draft preparation, X.X. and S.H.; writing—review and editing, F.L. and B.Z.; visualization, X.X.; supervision, F.L. and D.G.; project administration, F.L. and D.G. All authors have read and agreed to the published version of the manuscript.

Funding: This research was funded by China Postdoctoral Science Foundation (Grant No. 2019M651818) and the National Natural Science Foundation of China (Grant No. 51878660).

Institutional Review Board Statement: Not applicable.

Informed Consent Statement: Not applicable.

Data Availability Statement: The data that support the findings of this study are available from the corresponding author upon reasonable request.

Conflicts of Interest: The authors declare no conflict of interest.

References

- Na, R.; Shen, Z.G. Assessing cooling energy reduction potentials by retrofitting traditional cavity walls into passively ventilated cavity walls. *Build. Simul.* **2021**, *14*, 1295–1309. [[CrossRef](#)]
- Ahmadi, J.; Mahdavinejad, M.; Larsen, O.K.; Zhang, C.; Zarkesh, A.; Asadi, S. Evaluating the different boundary conditions to simulate airflow and heat transfer in Double-Skin Facade. *Build. Simul.* **2022**, *15*, 799–815. [[CrossRef](#)]
- Nardi, I.; Lucchi, E.; de Rubeis, T.; Ambrosini, D. Quantification of heat energy losses through the building envelope: A state-of-the-art analysis with critical and comprehensive review on infrared thermography. *Build. Environ.* **2018**, *146*, 190–205. [[CrossRef](#)]
- Nardi, I.; Paoletti, D.; Ambrosini, D.; de Rubeis, T.; Sfarra, S. U-value assessment by infrared thermography: A comparison of different calculation methods in a Guarded Hot Box. *Energy Build.* **2016**, *122*, 211–221. [[CrossRef](#)]
- Bouchair, A. External environmental temperature: Proposed new formulation. *Build. Serv. Eng. Res. Technol.* **2001**, *22*, 133–156. [[CrossRef](#)]
- McAdams, W.H. *Heat Transmission*; McGraw-Hill Kogakusha: Tokyo, Japan, 1954.
- Jürges, W. Der wärmeübergang an einer ebenen wand (heat transfer at a plane wall). *Gesundh.-Ing.* **1924**, *1*, 105.

8. Sparrow, E.M.; Ramsey, J.W.; Mass, E.A. Effect of finite width on heat transfer and fluid flow about an inclined rectangular plate. *J. Heat Transf.* **1979**, *101*, 199–204. [[CrossRef](#)]
9. Jayamaha, S.E.G.; Wijesundera, N.E.; Chou, S.K. Measurement of the heat transfer coefficient for walls. *Build. Environ.* **1996**, *31*, 399–407. [[CrossRef](#)]
10. Sturrock, N.S. Localised Boundary Layer Heat Transfer from External Building Surfaces. Ph.D. Thesis, University of Liverpool, Liverpool, UK, 1971.
11. Ito, N.; Kimura, K.; Oka, J. Field experiment study on the convective heat transfer coefficient on exterior surface of a building. *ASHRAE Trans.* **1972**, *78*, 184–191.
12. Nicol, K. The energy balance of an exterior window surface, Inuvik, NWT, Canada. *Build. Environ.* **1977**, *12*, 215–219. [[CrossRef](#)]
13. Yazdaniyan, M.; Klems, J.H. Measurement of the exterior convective film coefficient for windows in low-rise buildings. *ASHRAE Trans.* **1994**, *100*, 1087–1096.
14. Loveday, D.L.; Taki, A.H. Convective heat transfer coefficients at a plane surface on a full-scale building facade. *Int. J. Heat Mass Transf.* **1996**, *39*, 1729–1742. [[CrossRef](#)]
15. Hagishima, A.; Tanimoto, J. Field measurements for estimating the convective heat transfer coefficient at building surfaces. *Build. Environ.* **2003**, *38*, 873–881. [[CrossRef](#)]
16. Yamamoto, T.; Ozaki, A.; Kaoru, S.; Taniguchi, K. Analysis method based on coupled heat transfer and CFD simulations for buildings with thermally complex building envelopes. *Build. Environ.* **2021**, *191*, 107521. [[CrossRef](#)]
17. Defraeye, T.; Blocken, B.; Carmeliet, J. Convective heat transfer coefficients for exterior building surfaces: Existing correlations and CFD modelling. *Energy Convers. Manag.* **2021**, *52*, 512–522. [[CrossRef](#)]
18. Fakhim, H.A.; Zamzaman, K.; Hanifi, M. Investigating the Effect of Different Parameters on CHTC Using Wind-Tunnel Measurement and Computational Fluid Dynamics (CFD) to Develop CHTC Correlations for Mixed CHTCS. *J. Mech.* **2020**, *36*, 915–932. [[CrossRef](#)]
19. Chen, S.; Mihara, K.; Wen, J. Time series prediction of CO₂, TVOC and HCHO based on machine learning at different sampling points. *Build. Environ.* **2018**, *146*, 238–246. [[CrossRef](#)]
20. Yi, Q.; Zhang, G.; Amon, B.; Hempel, S.; Janke, D.; Saha, C.K.; Amon, T. Modelling air change rate of naturally ventilated dairy buildings using response surface methodology and numerical simulation. *Build. Simul.* **2021**, *14*, 827–839. [[CrossRef](#)]
21. Tominaga, Y.; Stathopoulos, T. CFD Simulations of Near-field Pollutant Dispersion with Different Plume Buoyancies. *Build. Environ.* **2018**, *131*, 128–139. [[CrossRef](#)]
22. Mochida, A.; Tominaga, Y.O.; Murakami, S.; Yoshie, R.; Ishihara, T.; Ooka, R. Comparison of various k-models and DSM applied to flow around a high-rise building—Report on AIJ cooperative project for CFD prediction of wind environment. *Wind. Struct.* **2002**, *5*, 227–244. [[CrossRef](#)]
23. ANSYS. *ANSYS 19 Fluent Theory Guide*; ANSYS: Canonsburg, PA, USA, 2018.
24. Huang, Y.D.; Xu, N.; Ren, S.Q.; Qian, L.B.; Cui, P.Y. Numerical investigation of the thermal effect on flow and dispersion of rooftop stack emissions with wind tunnel experimental validations. *Environ. Sci. Pollut. Res.* **2021**, *28*, 11618–11636. [[CrossRef](#)]
25. Vapnik, V. *The Nature of Statistical Learning Theory*, 2nd ed.; Springer: Berlin/Heidelberg, Germany, 1999.
26. Hsu, C.W.; Chang, C.C.; Lin, C.J. A Practical Guide to Support Vector Classification. *Dep. Comput. Sci.* **2003**, *106*, 1396–1411.